

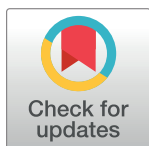
RESEARCH ARTICLE

Efficient removal of toxic azo dyes from contaminated water by adsorption on the GO surface

Haris bin Tanveer¹, Fouzia Perveen^{1*}, Sumaiya Azam¹, Nasima Arshad², Hummera Rafique³, Ahmad Irfan⁴, Zoniya Arshad³, Salman u Zaman¹, Sher Qadar²

1 School of Interdisciplinary Engineering & Sciences (SINES), National University of Sciences & Technology (NUST), Islamabad, Pakistan, **2** Department of Chemistry, Allama Iqbal Open University, Islamabad, Pakistan, **3** Department of Chemistry, University of Gujrat, Gurjat, Pakistan, **4** Department of Chemistry, College of Science, King Khalid University, Abha, Saudi Arabia

* fouzia@sines.nust.edu.pk



Abstract

The purpose of this study is to examine the possibility of GO to be used as an adsorbent for five novel potentially hazardous azo-dyes for their removal from aqueous solution. Adsorption characteristics of GO for azo-dyes removal were investigated by means of experimental and computational DFT as well as Monte Carlo approaches. Experimental studies include the effect of adsorbent dose, contact time, and initial concentration, while computational investigation involves DFT and Monte Carlo (MC) simulations. Through DFT studies geometric, electronic, and thermodynamic parameters were explored and possible mechanism of interactions and adsorption energies by predicted through MC by searching lowest possible adsorption complexes. Experimental data were evaluated by Langmuir models in order to describe the equilibrium isotherms. Equilibrium data fitted well to the Langmuir model. Thermodynamic parameters i.e., free energy change, enthalpy change, and entropy change revealed that the removal of azo-dyes by adsorption on the surface of GO molecular sieves was spontaneous. Nature of the process was found to be physisorption involving non-covalent interaction. The study unveiled that GO can be used as an efficient adsorbent material for the adsorption of azo-dyes from aqueous solution.

OPEN ACCESS

Citation: Tanveer Hb, Perveen F, Azam S, Arshad N, Rafique H, Irfan A, et al. (2024) Efficient removal of toxic azo dyes from contaminated water by adsorption on the GO surface. PLoS ONE 19(3): e0299364. <https://doi.org/10.1371/journal.pone.0299364>

Editor: Avvaru Praveen Kumar, Adama Science and Technology University, ETHIOPIA

Received: October 14, 2023

Accepted: February 8, 2024

Published: March 29, 2024

Copyright: © 2024 Tanveer et al. This is an open access article distributed under the terms of the [Creative Commons Attribution License](https://creativecommons.org/licenses/by/4.0/), which permits unrestricted use, distribution, and reproduction in any medium, provided the original author and source are credited.

Data Availability Statement: All relevant data are within the manuscript and its [Supporting Information](#) files.

Funding: The author(s) received no specific funding for this work.

Competing interests: The authors declare that they have no conflicts of interest or any competing interest.

1. Introduction

Now a days over 10,000 dyes are being used in various industries including leather, plastics, rubber, cosmetic, textile, paper, food and pharmaceutical industries [1]. The release of these dyes into water is responsible for reduced photosynthetic activity due to interference with transmission of sunlight [2]. For the purpose of making color long-lasting, these dyes are designed to resist decomposition with time, exposure to sunlight, water and soap. Due to their complex structure, dyes cannot be easily removed from water by conventional wastewater treatment processes [3].

Azo dyes are organic compounds having aryl functional group. Wastewater released from factories has high percentage of Azo dyes dissolved in it which not only damage plant growth

but causes metabolic stress and neurosensory damage in fish [4]. Azo dyes can come in contact with humans through a number of ways. Approx. 4-5% of azo dyes decompose to form aromatic amines, which are potentially cancerous and have therefore been regulated. Specifically, they have been seen to cause bladder and liver cancers [5]. Adsorption is a robust, well studied, widely employed and promising water treatment method which is considered to be one of the most simple and economical to remove the dyes from sewages [6]. The adsorption attempts have been made to find alternative low-cost adsorbents [7].

In the last decade, nanocarbon based adsorbents have attained much attention in water treatment. These adsorbents are synthesized from low-cost materials and are proven to be highly efficient than other adsorbents. One widely used and known adsorbent material is activated carbon. Carbon nanotubes (CNT), characterized by hollow tubular structure with high surface area, have also been studied for the adsorption of a large number of different organic compounds from water [8]. Now a days, graphene-based materials such as graphene oxide (GO) and reduced graphene oxide (rGO) have been widely investigated for adsorption application [9–13]. Graphene based materials have high surface area compared to CNT and consist of sp² and sp³ hybridized hexagonal honeycomb carbon network with abundant functional sites which are ideal for a proficient adsorbent material [14]. In GO, additionally surface defects such as vacancies and sp³ bonded atoms are most common [15]. The presence of these functional groups or defects allows GO to easily interact with organic and inorganic compounds by covalent or non-covalent interactions [16]. Moreover, GO has high dispersion ability in the aqueous solutions compared to graphite due to increased interplanar distance or weakened interplanar π - π interactions, the GO may regain sufficient conjugated structure of graphene which are vital for any adsorbents of organic dyes, particularly for aromatic structures [17, 18]. In one of our previous work, we presented a simple and facile method for the reduction of silver salt in the presence of GO using Azo dyes including EBT and MO for developing composites. Wojciech Konicki *et al.*, performed experimental studies for the removal of industrial acid Orange 8 (AO8) and Direct Red 23 (DR23) dyes by adsorption onto graphene oxide [19].

The aim of this work is to study the removal of five novel dyes which are released into water as a result of chemical laboratory synthesis. These dyes are classified as azo-dyes, and a majority of azodyes exhibit toxicity, carcinogenicity, and mutagenicity, leading to adverse effects such as allergies, dermatitis, skin irritation, cancer, and mutations in both humans and animals [20, 21].

We present here the removal of five novel azo dyes through graphene oxide as the adsorbent using both computational approaches and experimental UV-Vis spectroscopy. Computational methods play a crucial role in studying adsorption processes for water purification, offering several advantages that enhance our understanding of the process. In the realm of water purification through adsorption, these methods provide detailed insights into the molecular interactions between adsorbent materials and contaminants at the atomic level. For understanding the specific adsorption mechanisms, binding energies, and thermodynamics at the molecular scale, DFT and Monte Carlo simulations were performed to determine the adsorption energy of the dyes and efficiency of GO for water purification [22].

Experimentally, to comprehend the adsorption mechanism of azo-dyes onto graphene oxide, a comprehensive analysis of the equilibrium, kinetic, and thermodynamic data for adsorption was conducted by using UV-Vis spectroscopic investigation.

The kinetics and thermodynamics of the adsorption were also measured by using both computational and experimental approaches. The nature of adsorption was explored to ensure recycling of the graphene oxide surface. To the best of our knowledge, computational prediction and then experimental validation for the adsorptive removal of these novel dyes on GO surface through diverse computational and experimental approaches is reported for the first time.

2. Materials and methods

2.1 Synthesis of graphene oxide

In modified Hummer's method conc. HNO_3 and KMnO_4 were utilized to synthesize GO from graphite powder. It is a safer method with the reduced preparation time of GO. For the synthesis of expanded graphite, 30 ml of conc. H_2SO_4 was added into 250ml beaker and placed it on a hot plate for stirring, conc. HNO_3 was added dropwise, 15g of graphite were added, beaker was covered with a lid and solution was left soaked for three days. After 3 days entire mixture was transferred into 200ml deionized water for intercalation of graphite to get expanded graphite. The mixture was centrifuged for 30 mins, two layers were generated, upper layer was decanted while lower layer of black precipitate was warmed in oven at 70 degrees for 3–4 hrs. After heating the intercalation of graphite was obtained which is highly hydrophilic and effectively be oxidized.

Oxidation of expanded graphite was performed by the addition of KMnO_4 in the presence of conc. H_2SO_4 with continuous stirring. During this process 4g of expanded graphite was added in three intervals. The solution was placed in an ice bath and proceeded with stirring. This solution was then placed in an ice bath for controlling the sudden elevation in temperature. After 1 hour 375 ml of deionized water was added and placed it in the water bath at 90°C followed by addition of H_2O_2 for the removal of remnants of manganese. After addition of hydrogen peroxide, mixture was centrifuged at 6000rpm and washed with deionized water.

To this mixture 1ml of 1M solution HCl was added and repeatedly at deionized water to remove permanganate and manganese dioxide salts. This layer-by-layer washing is known as chemical exfoliation. Mixture was taken and placed on hot plate with stirring for 1hr. Now precipitates were dried at 60–70°C as dried precipitates of graphene oxide [23].

2.2 General method for synthesis of azo dyes

Amine-I (4,4'-methylene dianiline) was weighed in grams on weighing balance. The weighed amine were dissolved into 20ml of dry methanol in a round bottom flask. The flask was placed in the ice bath on stirring plate and by using the thermometer the temperature was maintained at 0–5°C. Then added the double moles of HCl in amount of 2ml on stirring and kept temperature at the range 0–5°C. NaNO_2 solution was prepared by weighed amount into the distilled water and was added drop wise into the reaction flask by using the dropper at the set temperature of 0–5°C. The contents of the reaction flask were stirred for 1hr till pink color appeared. Aldehyde (weighed amount) were added by making the solution of it into the required amount of Methanol keeping the temperature same. Put the aldehyde solution into the reaction flask drop wise at maintained temperature. Then allowed the reaction to stir for further 3hrs until color changed into orange brown shade. The reaction was monitored by TLC after completion, neutralized the solution at the same temperature by adding the sodium hydroxide (NaOH) solution drop wise. The precipitates were appeared and the reaction mixture was removed from the ice bath and filtered it. After washing precipitates were allowed the to dry. The general reaction for the synthesis of the Azo dyes from Amine-I is given in the [S1 Scheme](#).

In the present work following five azo dyes were synthesized by using above scheme as mentioned in [Fig 1](#).

2.3 UV-vis spectroscopic procedure

Adsorption studies for azo dyes have been carried out to investigate the effect of different parameters such as adsorbate concentration, adsorbent dose, solution containing various concentrations of adsorbate (ppm) and 0.05g adsorbent was taken in 100ml (1:9; DMSO: water)

IUPAC Names	Abbreviation Names	Structures
Bis 3,3'-(4,4'-Diazenyldiphenylmethane)-4-chlorobenzaldehyde	(HT-1)	
Bis 3,3'-(4,4'-Diazenyldiphenylmethane)-p-anisaldehyde	(HT-2)	
Bis 3,3'-(4,4'-Diazenyldiphenylmethane)-naphthaldehyde	(HT-3)	
Bis 3,3'-(4,4'-Diazenyldiphenylmethane)-salicylaldehyde	(HT-4)	
Bis 3,3'-(4,4'-Diazenyldiphenylmethane)-2,4-dihydroxybenzaldehyde	(HT-5)	

Fig 1. Molecular structures and IUPAC names of five novel azo dyes used as adsorbates.

<https://doi.org/10.1371/journal.pone.0299364.g001>

mixture in conical flask and agitated at 150rpm in orbital shaker. The initial and final azo-dyes concentrations remaining in solutions were analyzed by a UV spectrophotometer (Shimadzu-1800), monitoring the absorbance changes at a wavelength ranges 200-800nm. The equilibrium adsorption capacity was calculated from the relationship below [24].

$$q_e \left(\frac{mg}{g} \right) = \frac{C_i - C_e}{C_e} \times \frac{V}{m} \quad (1)$$

Where C_i and C_e are the initial and equilibrium concentrations of aniline in ppm, q is the adsorption capacity in mg/g, V is the volume of azo-dyes solution in L, and m is the adsorbent mass in g.

2.4 Quantum chemical DFT calculation

Quantum chemical density functional theory (DFT) studies were performed by using SCM-ADF modeling suite 2018.105 for the adsorption kinetic studies of five novel azo dyes on the surface of GO molecular sieves. X-ray crystallographic structure of GO was obtained, modelled, and imported to ADF graphical interface as adsorbent. Optimized structures of five azo-dyes were then adsorbed on the surface of GO to study electronic, kinetic, and thermodynamic effects of heterogeneous adsorption. All calculations were carried out using SCM-ADF [25] employing the generalized gradient approximation (GGA) due to Perdew-Burke Ernzerhof (PBE) exchange correlation [26]. The basis sets representing the electron density consist of both Hermene Skillman numerical atomic orbitals (NAOs) and Slater-type orbitals (STOs) with a frozen core. Scalar relativistic corrections were included through the zeroth order regular approximation [27]. A three-dimensional translational symmetry was implemented for the single layer of GO. In our computation, overall energy convergence was well within 0.1eV, at LDA-GGA level of theory. Adsorption energy was calculated to determine efficiency of azo dyes binding on the GO surface. Thermodynamic parameters calculated at temperature provided insight into stability of adsorbent in azo dye removal process.

2.5 Monte Carlo simulations

Molecular simulations were implemented using Material Studio for exploring adsorption mechanisms and interactions between azo dyes and graphene oxide. Firstly, azo dyes and graphene oxide were optimized using the Forcite module in Material Studio software. The energy setting was UNIVERSAL forcefield with fine quality. The obtained optimized structures then were used for studying adsorption mechanisms and to identify the lowest energy adsorption location of dyes on GO using the Adsorption Locator tool in Material Studio. This module works by performing Monte Carlo searches of configurational structures of the Dyes-GO complex as the T is gradually decreased. The Monte Carlo simulations were performed for 100 annealing cycles, with same energy setting as used in geometry optimization.

3. Result and discussion

3.1 Characterizations of graphene oxide (GO)

GO characterization was done by FT-IR, XRD, TGA, SEM, and UV-spectroscopy and the related spectrum and graphs are provided in [S1A–S1E Fig](#). In FT-IR of GO, the peak at 3200–3400 cm^{-1} indicated the O-H stretching groups, the peak at 1740.85 cm^{-1} recognized for C = O stretch, and a band at 1045.79 cm^{-1} indicated (epoxy) groups. In XRD, GO showed intensive sharp peak centered at $2\theta = 12.09^\circ$, corresponding to the (002) inter planar spacing of 0.74 nm. In TGA of GO, two step decomposition was observed. The first step (100–245.6°C) is due to oxygen containing functionalities i.e. –COOH, –OH, –C = O, while in the second step (245.6–707.5°C) degradation in graphitic backbone has occurred. A sheet like structure in SEM micrograph indicated the exfoliation phenomena of GO. UV- spectrum of GO showed peak at λ_{max} at 235 nm which could be attributed to the π - π electronic transition of aromatic groups, while a shoulder peak at 300 nm depicted the presence of carbonyl groups (C = O).

The low cost, recyclability, and stability are the key factors to ascribe the efficiency of a catalyst or adsorbent [28–30]. A recycle usage experiment was performed and dispersions were filtered, cleaned with deionized water, and dried. To ascertain the stability of recycled GO, its FTIR was done, and the spectrum showed no significant change, hence assured its stability to be re-used as an absorbent for fresh dye solution. The FTIR of used adsorbent (GO) is provided as [S1F Fig](#).

3.2 Characterization of synthetic azo dyes

All the synthesized Azo compounds were characterized by IR-spectroscopy, the overall range for different functionalities in IR spectra were interpreted. The characteristic peaks for aromatic C = C in IR were observed in the region from 1575–1610 cm^{-1} . The fundamental signals for Azo compounds -N = N were observed in the range from 1436–1478 cm^{-1} . The carbonyl C = O peaks were appeared in the region 1653–1684 cm^{-1} and the peaks for C-N functionality is observed in the range 1506–1516 cm^{-1} .

The structural confirmation was also carried out by ^1H and ^{13}C -NMR analysis. In the ^1H -NMR data of compounds (HT-1-5), the appearance of characteristic signals at 9.86–10.06 ppm for (aldehydic C = O) and 3.84–3.89 ppm for (Ar-CH₂) confirmed the synthesis of compounds of our interest. In the ^{13}C -NMR data the characteristic signals were observed at 198.4–199.6 ppm for (aldehydic C = O) and 44.3–44.9 ppm for (Ar-CH₂). Elemental analysis data and the appearance of characteristic signals in the FT-IR and NMR spectra confirmed the synthesis of our desired Azo compounds. Elemental analysis also indicate the successful synthesis of our target Azo compounds. Representative IR and NMR spectra for HT-2 are provided in [S2 Fig](#), whereas the data is provided as below.

Bis 3,3'-(4,4'-Diazenyldiphenylmethane)-4-chlorobenzaldehyde (HT-1). Color: Dark Red, Yield: 76%, melting point/decompose: 288–290°C.; IR (KBr, ν_{\max}): 1589 (C = C), 1436 (N = N), 1659 (C = O), 1514 (C-N) cm^{-1} .; ^1H NMR (300 MHz, CDCl_3 , δ ppm): 9.93 (2H, s, -CHO), 8.61 (4H, d, $J = 7.6$ Hz, Ar-H-1'), 8.17 (2H, d, $J = 2.4$ Hz, H-2), 8.07 (2H, dd, $J = 7.4, 2.4$ Hz, H-6), 7.86 (2H, dd, $J = 7.4$ Hz, H-5), 7.54 (4H, d, $J = 7.6$ Hz, Ar-H-2'), 3.88 (-CH₂).; ^{13}C NMR (75 MHz, CDCl_3 , δ ppm): 198.4 (aldehydic C = O), 154.2 (C-3,3), 152.5 (C-3'3'), 145.7 (C-4',4'), 136.5 (C-4,4), 133.4 (C-1,1), 131.3 (C-6,6), 129.1 (C-5,5), 128.2 (C-2,2), 125.4 (2xC-1',1'), 124.2 (2xC-2',2'), 44.3 (-CH₂).; Anal. Calcd for C₂₇H₁₈N₄O₂Cl₂ (500): C, 64.68; H, 3.62; N, 11.17; Found: C, 64.64; H, 3.57; N, 11.19%.

Bis 3,3'-(4,4'-Diazenyldiphenylmethane)-*p*-anisaldehyde (HT-2). Color: Brown, Yield: 75%, melting point/decompose: 190–192°C.; IR (KBr, ν_{\max}): 1597 (C = C), 1449 (N = N), 1670 (C = O), 1507 (C-N) cm^{-1} .; ^1H NMR (300 MHz, CDCl_3 , δ ppm): 9.88 (2H, s, -CHO), 8.57 (4H, d, $J = 7.6$ Hz, Ar-H-1'), 8.21 (2H, d, $J = 2.4$ Hz, H-2), 8.12 (2H, dd, $J = 7.4, 2.4$ Hz, H-6), 7.78 (2H, dd, $J = 7.4$ Hz, H-5), 7.64 (4H, d, $J = 7.6$ Hz, Ar-H-2'), 3.92 (-OCH₃), 3.87 (-CH₂).; ^{13}C NMR (75 MHz, CDCl_3 , δ ppm): 198.2 (aldehydic C = O), 154.7 (C-3,3), 153.4 (C-3'3'), 146.3 (C-4',4'), 137.5 (C-4,4), 134.2 (C-1,1), 132.8 (C-6,6), 131.3 (C-5,5), 130.5 (C-2,2), 126.3 (2xC-1',1'), 124.7 (2xC-2',2'), 56.2 (-OCH₃), 44.6 (-CH₂).; Anal. Calcd for C₂₉H₂₄N₄O₄ (492): C, 70.72; H, 4.91; N, 11.38; Found: C, 70.74; H, 4.95; N, 11.36%.

Bis 3,3'-(4,4'-Diazenyldiphenylmethane)naphthaldehyde (HT-3). Color: Orange, Yield: 62%, melting point/decompose: 180–182°C.; IR (KBr, ν_{\max} , cm^{-1}): 1575 (C = C), 1457 (N = N), 1684 (C = O), 1507 (C-N) cm^{-1} .; ^1H NMR (300 MHz, CDCl_3 , δ ppm): 9.91 (2H, s, -CHO), 8.87 (4H, d, $J = 7.6$ Hz, Ar-H-1'), 8.76–7.68 (12H, m, Ar), 7.61 (4H, d, $J = 7.6$ Hz, Ar-H-2'), 3.86 (-CH₂).; ^{13}C NMR (75 MHz, CDCl_3 , δ ppm): 198.8 (aldehydic C = O), 152.4 (C-3'3'), 148.7 (C-3,3), 145.4 (C-4',4'), 138.4 (C-4,4), 137.5 (C-1,1), 134.6 (C-10,10), 133.2 (C-9,9), 132.5 (C-2,2), 131.4 (C-5,5), 130.5 (C-6,6), 129.7 (C-7,7), 128.5 (C-8,8), 127.4 (2xC-1',1'), 125.6 (2xC-2',2'), 44.5 (-CH₂).; Anal. Calcd for C₃₅H₂₄N₄O₂ (532): C, 78.93; H, 4.54; N, 10.52; Found: C, 78.97; H, 4.55; N, 10.53%.

Bis 3,3'-(4,4'-Diazenyldiphenylmethane)salicylaldehyde (HT-4). Color: Brown, Yield: 68%, melting point/decompose: 198–200°C.; IR (KBr, ν_{\max}): 1598 (C = C), 1478 (N = N), 1653 (C = O), 1506 (C-N) cm^{-1} .; ^1H NMR (300 MHz, CDCl_3 , δ ppm): 10.03 (2H, s, -CHO), 8.66 (4H, d, $J = 7.6$ Hz, Ar-H-1'), 8.26 (2H, dd, $J = 7.4, 2.3$ Hz, H-4), 7.96 (2H, dd, $J = 7.4, 2.4$ Hz, H-6), 7.81 (2H, dd, $J = 7.4, 7.4$ Hz, H-5), 7.67 (4H, d, $J = 7.6$ Hz, Ar-H-2'), 5.46 (-OH), 3.86 (-CH₂).; ^{13}C NMR (75 MHz, CDCl_3 , δ ppm): 199.2 (aldehydic C = O), 158.5 (C-2,2), 154.8 (C-3,3), 153.6 (C-3'3'), 146.9 (C-4',4'), 138.3 (C-4,4), 136.6 (C-1,1), 134.1 (C-6,6), 132.7 (C-5,5), 126.8 (2xC-1',1'), 125.6 (2xC-2',2'), 44.7 (-CH₂).; Anal. Calcd for C₂₇H₂₀N₄O₄ (464): C, 69.82; H, 4.34; N, 12.06; Found: C, 69.88; H, 4.45; N, 12.03%.

Bis 3,3'-(4,4'-Diazenyldiphenylmethane)-2,4-dihydroxybenzaldehyde (HT-5). Color: Yellow, Yield: 68%, melting point/decompose: 178–180°C.; IR (KBr, ν_{\max}): 1610 (C = C), 1445 (N = N), 1683 (C = O), 1516 (C-N) cm^{-1} .; ^1H NMR (300 MHz, CDCl_3 , δ ppm): 10.06 (2H, s, -CHO), 8.83 (4H, d, $J = 7.4$ Hz, Ar-H-1'), 7.96 (2H, d, $J = 2.4$ Hz, H-4), 7.84 (2H, d, $J = 2.4$ Hz, H-6), 7.72 (4H, d, $J = 7.4$ Hz, Ar-H-2'), 5.48, 5.54 (-OH), 3.89 (-CH₂).; ^{13}C NMR (75 MHz, CDCl_3 , δ ppm): 199.6 (aldehydic C = O), 158.6 (C-2,2), 157.4 (C-4,4), 154.8 (C-3,3), 153.8 (C-3'3'), 137.3 (C-1,1), 134.5 (C-6,6), 133.7 (C-5,5), 127.4 (2xC-1',1'), 126.5 (2xC-2',2'), 44.9 (-CH₂).; Anal. Calcd for C₂₇H₂₀N₄O₆ (496): C, 65.32; H, 4.06; N, 11.29; Found: C, 65.37; H, 4.05; N, 11.33%.

3.3 Effect of adsorbent dosage on the adsorption capacity. The results of experiments to get insight into the effects of adsorbent dosage on the removal of each azo-dye removal are shown in Fig 2. UV-Vis spectroscopic representation depicted variation in absorbance and hence concentration of azo dyes upon GO addition [31]. Hypochromism in Fig 2A–2E

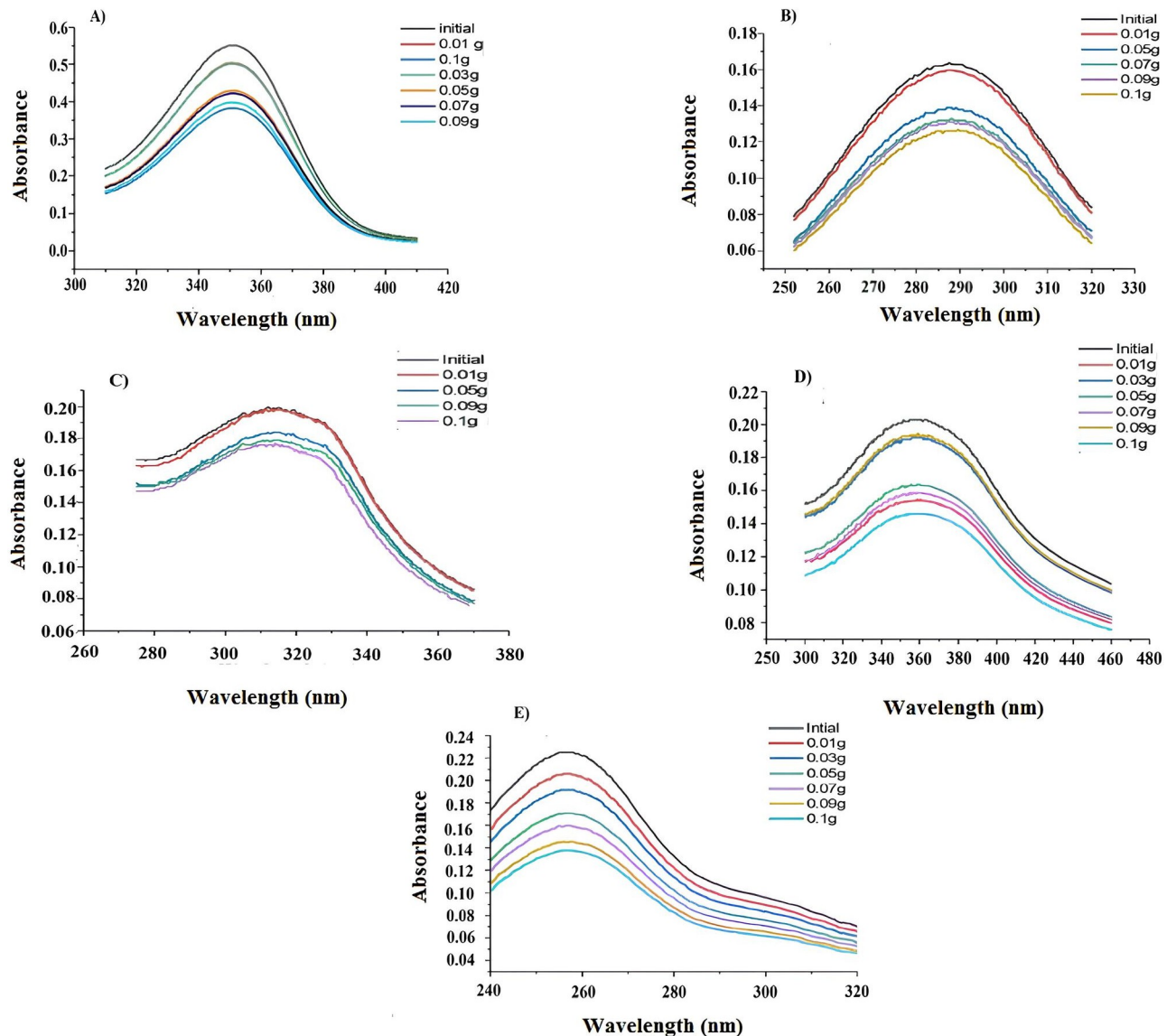


Fig 2. UV-Vis Spectral representation of the effect of Graphene Oxide dosage at a fixed concentration of azo-dyes A) (HT 1-1), B) (HT 1-2), C) (HT 1-3), D) (HT 1-4), and E) (HT 1-5) at 298K temperature.

<https://doi.org/10.1371/journal.pone.0299364.g002>

revealed that absorbance and hence concentration of azo dyes was decreased with increase in concentration of GO. However, a prompt decrease in concentration of azo dyes was observed at GO dosages ranging between 0.01g and 0.1g reflecting significant adsorption and hence interaction of azodyes with at specific dosage of GO. Increase of GO dosage above 0.05g had meager effect on the decrease in concentration of azo dyes indicative of the fact that azo dye removal efficiency is maximum for GO concentration between 0.01 and 0.1g and further increase in its concentration has not effect on azo dye removal.

It is apparent from Fig 1 that there was no shift in λ_{\max} demonstrating physisorption nature of the process. Physisorption is favorable for recycling GO after adsorption as it is attributed to the non-covalent interactions between GO and azo-dyes, hence making feasible removal of azodyes from water.

3.4 Effect of contact time and initial azo-dyes concentrations on the adsorption capacity

The effect of the initial concentration of azo-dyes on their removal rate at 0.05g GO dosage is represented in Fig 3. It is evident that the adsorption at different concentrations is fast at the initial stages and gently reduces with the progress of adsorption until the equilibrium is established. This indicated that saturation of GO surface reduced adsorption rate of azodyes and is increased after surface refreshing of GO which can be feasibly achieved due to physisorption. The amount of azo dyes adsorbed at equilibrium (q_e) was increased as the initial concentration of azodyes was enhanced at equilibrium. Therefore, a higher initial concentration of azo dyes improve the sorption process. The azo-dyes removal efficiency remained constant as the azo-dyes concentration was increased after equilibrium. Fig 3 also indicated that the adsorption

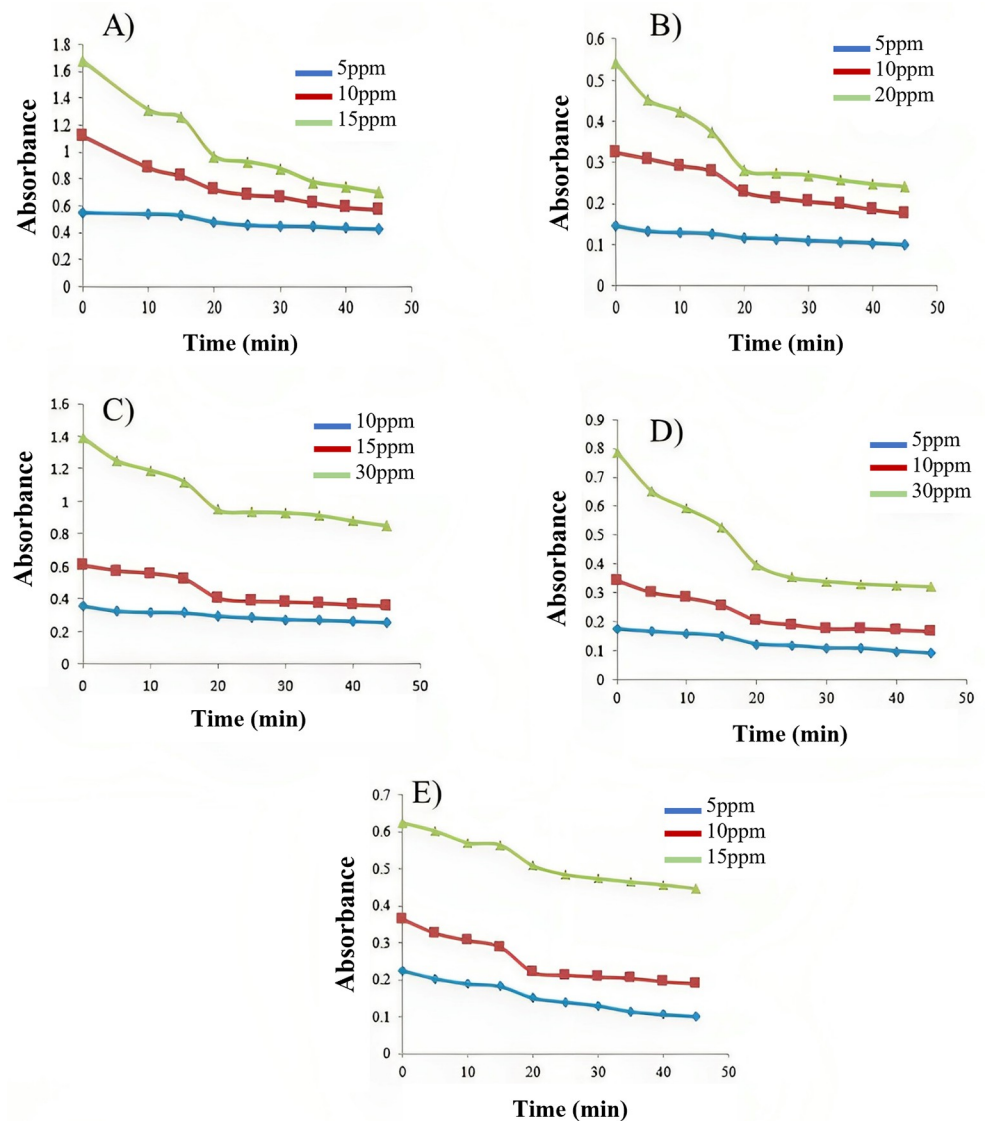


Fig 3. Graphical representation of Contact time study using 0.05g quantity of Graphene Oxide at various concentrations of azo-dyes A) (HT 1-1), B) (HT 1-2), C) (HT 1-3), D) (HT 1-4), and E) (HT 1-5) at 298K temperature by means of UV-Vis spectroscopy.

<https://doi.org/10.1371/journal.pone.0299364.g003>

process gradually increased with the increase of contact time and it stayed constant after adsorption equilibrium was acquired at about 20mins which is equilibrium time.

3.5 Adsorption isotherms

Equilibrium data, formally recognized as adsorption isotherms, have significant importance in the basic principles of adsorption processes, and are critical in optimizing the use of adsorbents

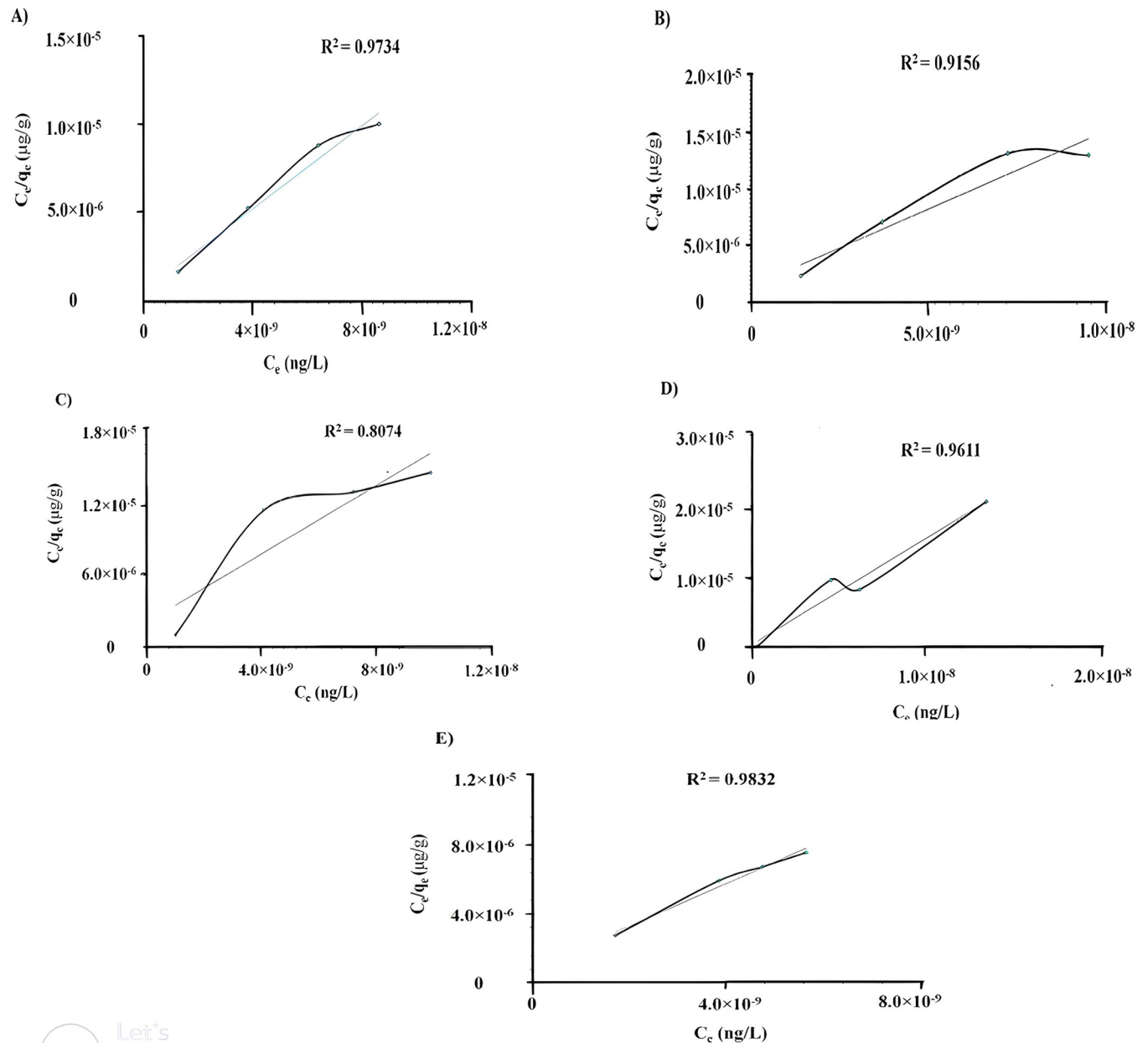


Fig 4. Graphical representation of Langmuir adsorption isotherm of adsorbed azo-dyes A) (HT 1-1), B) (HT 1-2), C) (HT 1-3), D) (HT 1-4), and E) (HT 1-5) on GO at 298K temperature using of UV-Vis spectroscopy.

<https://doi.org/10.1371/journal.pone.0299364.g004>

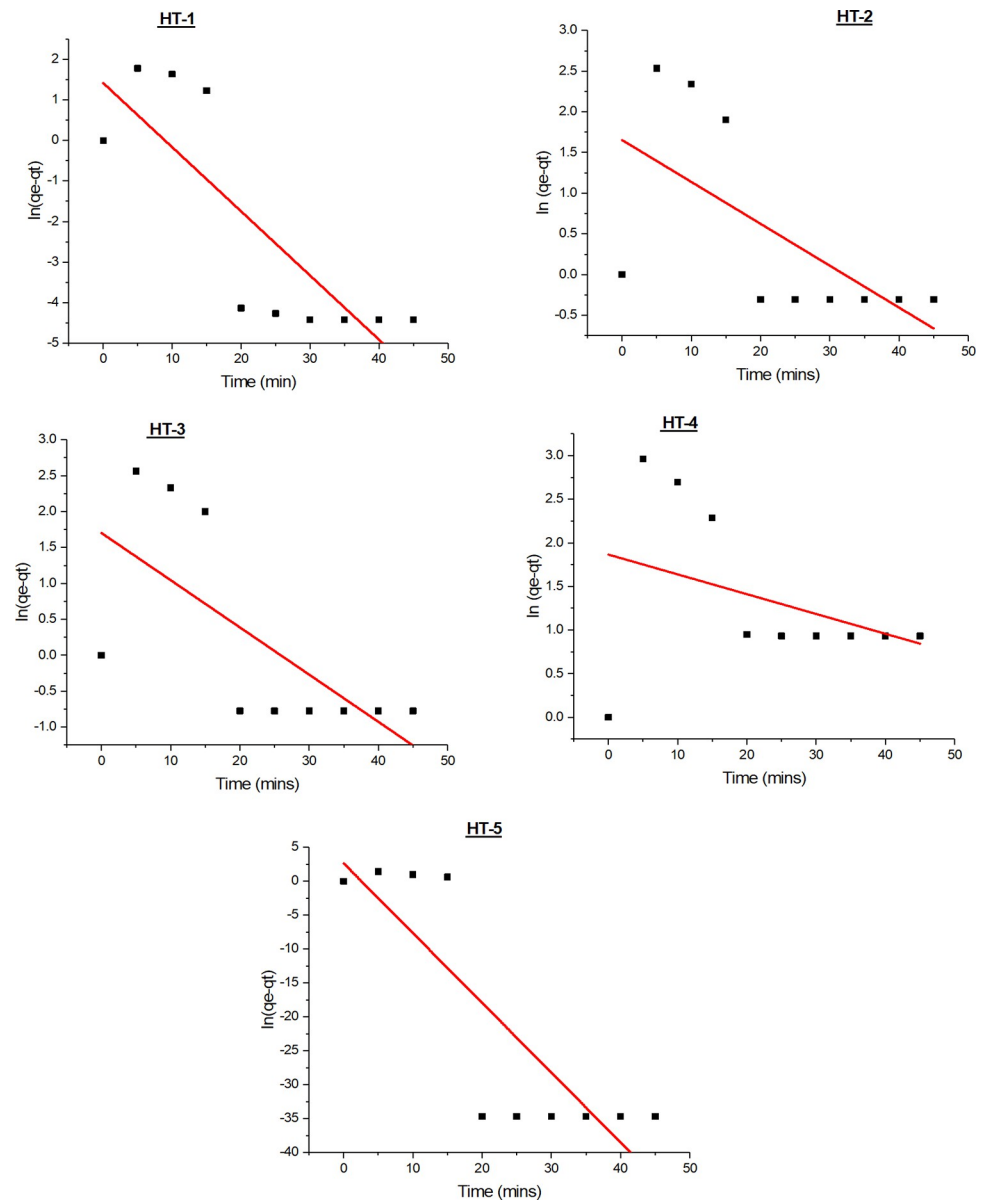


Fig 5. Pseudo-first-order kinetic modeling of azo-dyes adsorption on GO.

<https://doi.org/10.1371/journal.pone.0299364.g005>

[32]. To optimize the design of an adsorption system for removal of azodyes from solutions, it is essential to establish the most appropriate correlation for the equilibrium curves. For the examination of the controlling mechanisms of adsorption process, Langmuir adsorption isotherm model is used for the adsorption of molecules on solid surface forming a monolayer on the surface [33]. In this work, Langmuir adsorption isotherm was used for each azo-dye molecule to be adsorbed on GO surface and for finding K_L and this further utilized for finding the ΔG for spontaneity of reaction.

Fig 4. depicted the graphical representation of Langmuir adsorption equation (Eq 2) for all five novel azo-dyes on the surface of GO and revealed that Bis 3,3'-(4,4'-Diazenyldiphenylmethane)-salicylaldehyde (HT-4) has highest Langmuir adsorption constant and hence strongest adsorption on the surface of GO because of intermolecular interaction of its -OH and

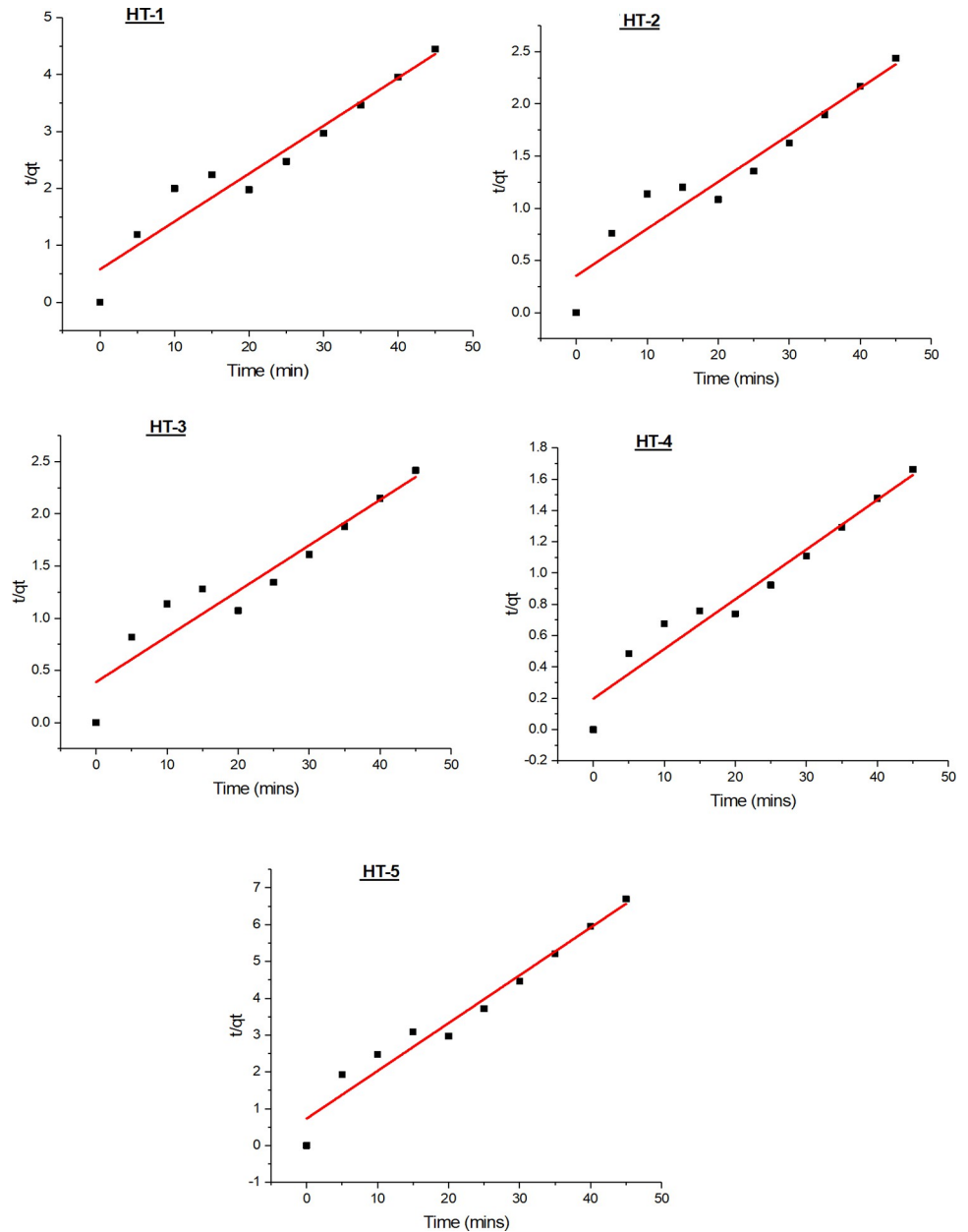


Fig 6. Pseudo-second-order kinetic modeling of azo-dyes adsorption on GO.

<https://doi.org/10.1371/journal.pone.0299364.g006>

-CHO groups coupler with graphene oxide-COC- group.

$$\frac{C_e}{q_e} = \frac{1}{K_L q_m} + \frac{C_e}{q_m} \tag{2}$$

Where, C_e = equilibrium concentration (mg/L), q_e = amount adsorbed per unit weight of adsorbent, K_L = Langmuir adsorption constant, q_m = maximum adsorbed amount.

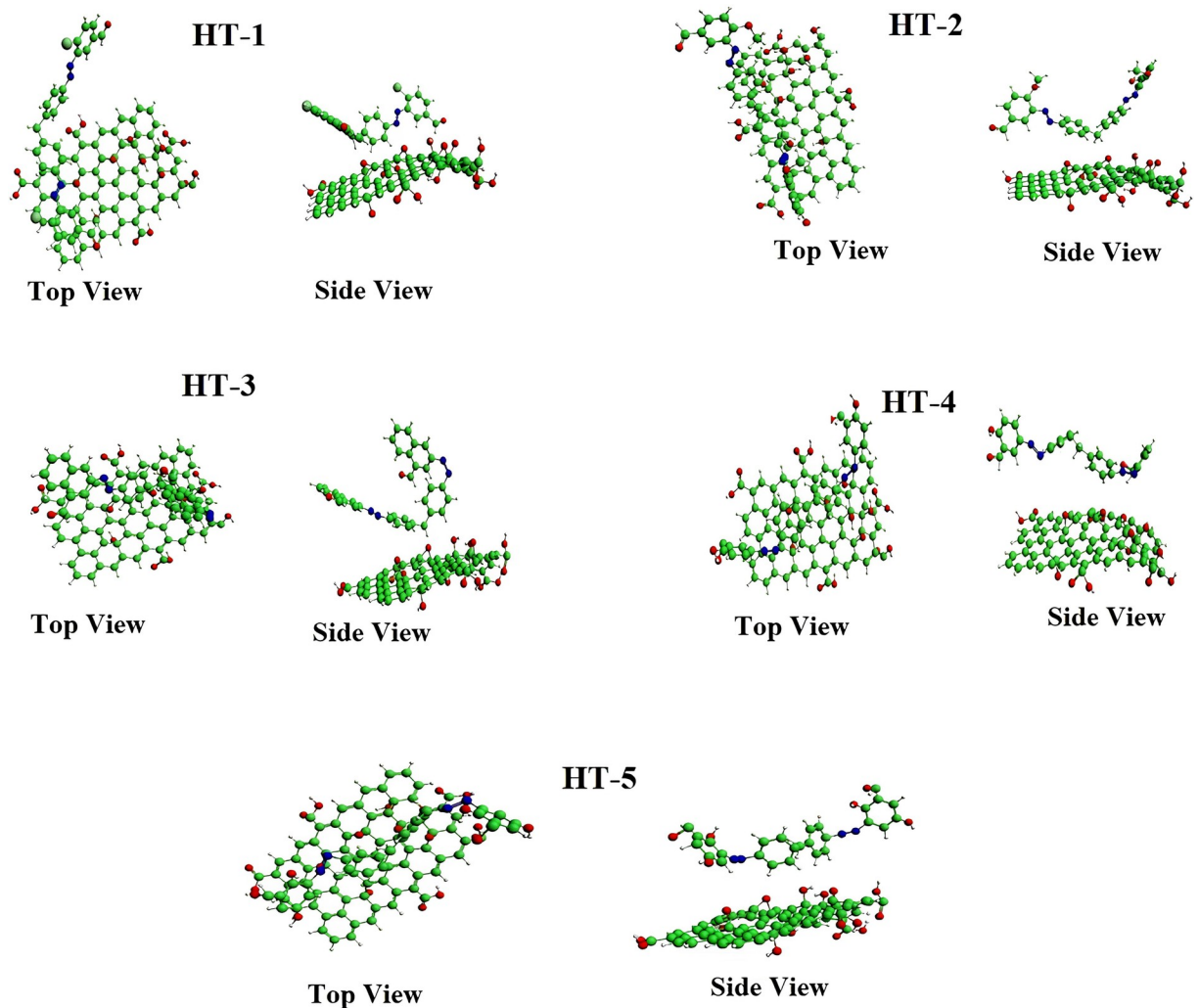


Fig 7. Top view and side view of optimized geometries of GO surface with adsorbed azodyes calculated through DFT studies at LDA-GGA:PBE level of theory.

<https://doi.org/10.1371/journal.pone.0299364.g007>

3.6 Adsorption kinetics

Various models can be employed to initiate the understanding of the solute adsorption process onto an adsorbent. Research efforts are undertaken to develop a rapid and efficient model for the design, focusing on the adsorption rate. For monitoring the process of adsorption, kinetics models were used to explain experimental data.

3.6.1 Pseudo-first-order kinetic model. The rate constant for the adsorption of dyes is represented by the pseudo-first-order kinetic model according to the Eq (3) as proposed by [34].

$$\ln(q_e - q_t) = \ln(q_e) - k_1 t \quad (3)$$

Here, q_e and q_t are the amounts of adsorbate adsorbed (mg/g) at equilibrium and at any instant of time t (min), respectively, k_1 is the rate constant of pseudo-first-order adsorption (min^{-1}). For Pseudo first order model, k_1 and q_e values were determined from the slope and intercept of the eq(3) as indicated in the Fig 5.

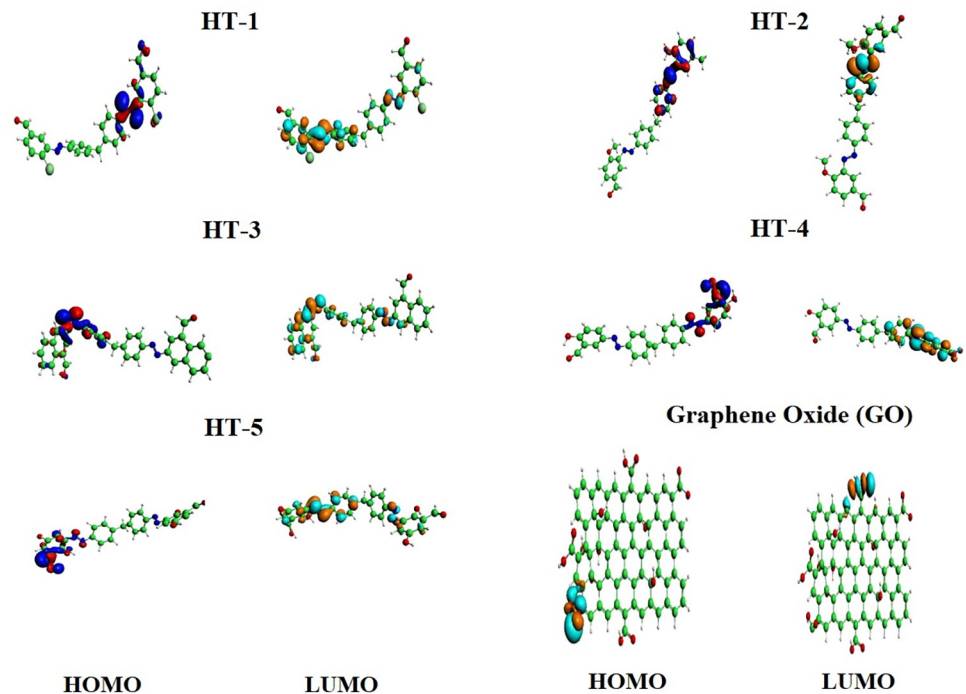


Fig. 8

Fig 8. Frontier molecular orbital analysis of azo dyes adsorbed showing distribution of isodensities indicating their reactive parts of azo dyes.

<https://doi.org/10.1371/journal.pone.0299364.g008>

3.6.2 Pseudo-second-order kinetic model. Based on equilibrium adsorption, the pseudo-second-order kinetic model, can be represented in the form as below.

$$\frac{t}{q_t} = \frac{1}{k_2 q_e^2} + \frac{t}{q_e}$$

where k_2 is the equilibrium rate constant of pseudo-second-order adsorption ($\text{g}/(\text{mg min})$). A plot of t/q_t vs. t (Fig 6) provides a linear relationship, rendering q_e and k_1 from the slope and intercept of the plot, respectively. Experimental data used for the Pseudo-first-order and second-order kinetic models has been provided as [S1 Table](#).

3.7 Computational methods and models

3.7.1 Quantum chemical DFT calculation. Computational quantum mechanical DFT studies were performed for finding the kinetics and mode of adsorption as well as nature of adsorption (physisorption or chemisorption) of azodyes. In one of our previous studies, DFT studies have been used for the comprehensive understanding of energetics and electron transfer mechanism of silver capped rGO for the photocatalytic degradation of EBT and MO. In this work, DFT simulations revealed that nature of adsorption of water contaminant azo dyes on the surface of GO was physisorption (Fig 7) as evident from top-view and side-view of dyes on the GO surface. Using an advanced DFT approach the adsorption energy was calculated with excellent accuracy.

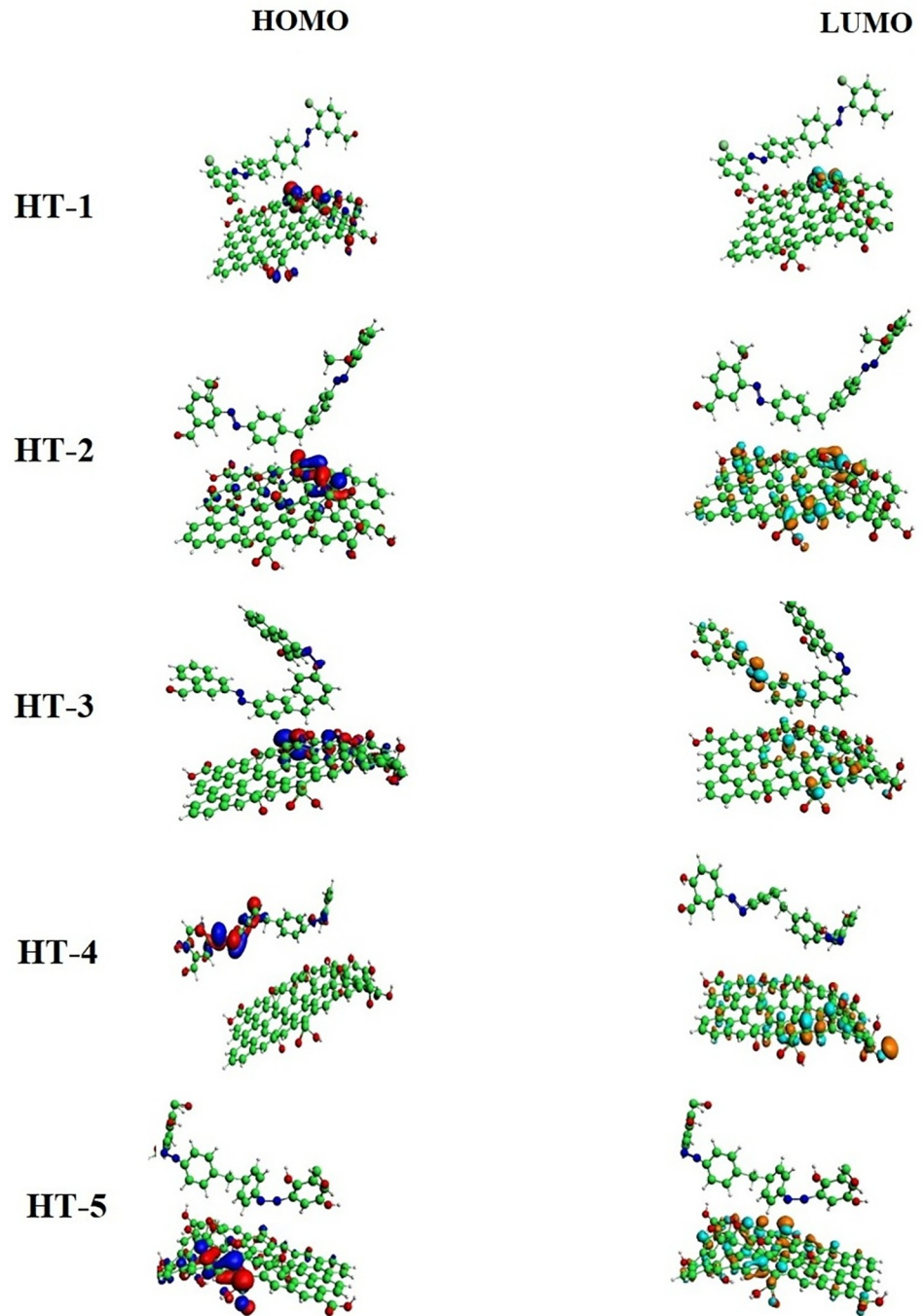


Fig 9. Frontier molecular orbital analysis of azo dyes adsorbed on GO surface showing distribution of HOMO and LUMO isodensities on GO and azo dyes.

<https://doi.org/10.1371/journal.pone.0299364.g009>

Energies of frontier molecular orbitals *i.e.*, E_{HOMO} and E_{LUMO} along with their isodensities distributions were calculated to monitor electrophilic or nucleophilic character of GO surface while acting as adsorbent. As evident from the Figs 8 and 9 that most distribution of HOMO isodensities are located on $\text{-C}=\text{O}$ part of GO reflecting its electron donating behavior while interacting with HT-1, HT-2, HT-3 and HT-5. However, for HT-4, HOMO isodensities are

Table 1. Adsorption distances, frontier orbital energies (E_{HOMO} , E_{LUMO}) and $\Delta E = E_{\text{HOMO}} - E_{\text{LUMO}}$ showing electronic interactions after adsorption.

Adsorption	Distance (Å)	E_{HOMO} kcal/mol	E_{LUMO} kcal/mol	$\Delta E = E_{\text{HOMO}} - E_{\text{LUMO}}$ kcal/mol
(HT-1)+GO	3.5	-134.45	-133.67	0.77
(HT-2)+GO	3.5(317–318)	-74.73	-72.91	1.82
(HT-3)+GO	3.5(313–314)	-111.61	-103.65	7.95
(HT-4)+GO	3.5(324–325)	-53.59	-51.96	1.63
(HT-5)+GO	3.5(314–315)	-82.60	-81.54	1.06

<https://doi.org/10.1371/journal.pone.0299364.t001>

Table 2. Comparison of Gibb's free energy (ΔG) and adsorption constant calculated from experimental and computational results.

Azo dye adsorption	Computational DFT data		Experimental data	
	$K_{\text{ad}}(\text{M}^{-1})$	Gibbs Free Energy (ΔG) kJ/mol	$K_{\text{L}}(\text{M}^{-1})$	Gibbs Free Energy (ΔG) kJ/mol
(HT-1) + GO	1.13×10^{10}	-57.37	1.94×10^9	-52.99
(HT-2) + GO	1.53×10^9	-52.41	1.37×10^9	-52.13
(HT-3) + GO	2.42×10^5	-30.72	7.08×10^8	-50.49
(HT-4) + GO	1.93×10^{10}	-58.69	3.76×10^9	-54.62
(HT-5) + GO	8.74×10^8	-51.01	1.55×10^9	-52.43

<https://doi.org/10.1371/journal.pone.0299364.t002>

distributed over HT-4 instead of GO, whereas LUMO isodensities are spread over all the GO surface indicative of strong electron accepting behavior of GO in the presence of HT-4 as adsorbate. For comprehensive understanding of electron transfer feasibility from E_{HOMO} to E_{LUMO} , ΔE ($E_{\text{HOMO}} - E_{\text{LUMO}}$ gap) was determined as depicted in Table 1.

Distribution of isodensities of azodyes were determined to assess their comparative reactivity. Smaller HOMO-LUMO gap implies feasible electrons transfer from E_{HOMO} to E_{LUMO} and hence maximum greater possibility of the interactions as revealed by Table 1. It was observed that HOMO-LUMO gap for azo dyes HT-1, HT-2, HT -4 and HT 1–5 was significantly smaller indicating greater electronic overlapping at distance of 3.5 Å while azo dye HT-3 showed comparatively larger HOMO-LUMO gap was high *i.e.*, -7.95 kcal/mol hence lesser reactivity as because of its stable 1-naphthoaldehyde coupler.

To probe into the fact that adsorption is thermodynamically favorable or not, thermodynamic parameters (ΔG , ΔH and ΔS) were calculated based on frequency calculation using GGA: PBE and electron correlation approximations. Table 2 tabulates thermodynamic parameters for five azodyes adsorbed at the distance of 3.5 Å on the surface of GO. A negative value of ΔG and ΔH represented that adsorption of all dyes on GO surface is thermodynamically favored and feasible. To find out strength of molecular interaction with azodyes and GO surface, adsorption constant K_{ad} was evaluated and indicated in Table 2. Computational data revealed that K_{ad} values for HT-4 was found to be highest due to its coupler. *i.e.* 2-hydroxybenzaldehyde. Coupler formed strong intermolecular interaction between its -OH, -CHO with -COC- group of GO. These trend are consistent with experimental results which showed highest value of K_{L} for HT-4. On the other hand, HT-3 furnished lowest affinity of adsorption on the surface of GO as compared to other azo dyes, because of very stable, conjugated and aromatic 1-naphthaldehyde coupler. Moreover, ΔG also revealed that azo dye HT-4 has greater spontaneity and HT-3 has least spontaneity as evident in Table 3.

The movement of water molecules and azo dyes from the GO molecular sieves hexagonal structure was determined by frequency calculations. The result revealed that water can easily passed through hexagon of GO due to small size of water molecule which is 1.63 Å width while GO hexagon has 2.87 Å. On the other hand, azo dyes are large sized 19.18 Å approximately and unable to pass through 2.78 Å hexagon as shown in Fig 10.

Table 3. Kinetics and thermodynamic parameter of adsorption at 3.5Å distance between azo dyes (HT 1-1), (HT 1-2), (HT 1-3), (HT 1-4), (HT 1-5) and graphene oxide at temperature 298K calculated using DFT.

Adsorption	Enthalpy	Entropy	Heat Capacity	Gibbs Free Energy	K_{ad} (M^{-1})
	ΔH (kJ/mol)	ΔS (kJ/mol-K)	C_v (kJ/K)	ΔG (kJ/mol)	
(HT-1)+GO	182.13	0.83	0.61	-57.37	1.13×10^{10}
(HT-2)+GO	164.7	0.79	0.55	-52.41	1.51×10^9
(HT-3)+GO	55.73	0.5	0.184	-30.72	2.42×10^5
(HT-4)+GO	187.02	0.83	0.64	-58.69	1.93×10^{10}
(HT-5)+GO	125.89	0.66	0.42	-51.01	8.74×10^8

<https://doi.org/10.1371/journal.pone.0299364.t003>

Interaction of azo-dyes and GO resulted in Vander Waal's interactions with no chemical bond formation, thus demonstrating that azo dyes adsorbed on the surface of GO *via* physisorption. Due to physisorption of azo dyes on GO, it can easily be recycled through desorption mechanism. Both experimental and computational results revealed that the azo-dye namely Bis 3,3'-(4,4'-Diazenyldiphenylmethane)-naphthaldehyde (HT-3) had lowest adsorption constant values due to intramolecular π - π interaction between its coupler rings; while the azo-dye namely, Bis 3,3'-(4,4'-Diazenyldiphenylmethane)-salicylaldehyde (HT-4) had highest adsorption constant values due to -OH and -COC-group of GO.

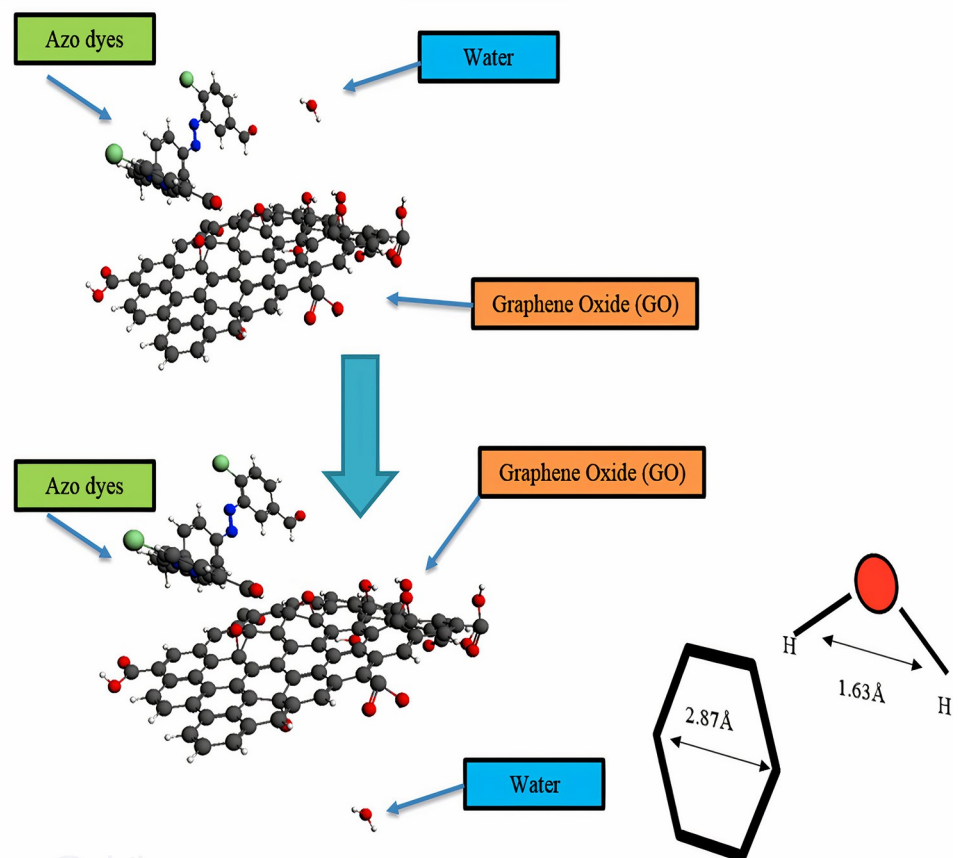


Fig 10. Passage of water molecules through graphene hexagon leaving behind large sized azo dyes; Graphene is acting as molecular sieve.

<https://doi.org/10.1371/journal.pone.0299364.g010>

Table 4. Calculated energies of adsorption complex of dyes and GO.

Total Energy (Kcal/mol)	185.0328
Adsorption Energy (Kcal/mol)	-178.1723
Rigid Adsorption Energy(Kcal/mol)	-184.5230
Deformation Energy(Kcal/mol)	6.3507
HT-1	-45.6128
dE_{ad}/dN_i (Kcal/mol)	
HT-2	-44.2370
dE_{ad}/dN_i (Kcal/mol)	
HT-3	-51.7192
dE_{ad}/dN_i (Kcal/mol)	
HT-4	-67.5352
dE_{ad}/dN_i (Kcal/mol)	
HT-5	-34.7123
dE_{ad}/dN_i (Kcal/mol)	

<https://doi.org/10.1371/journal.pone.0299364.t004>

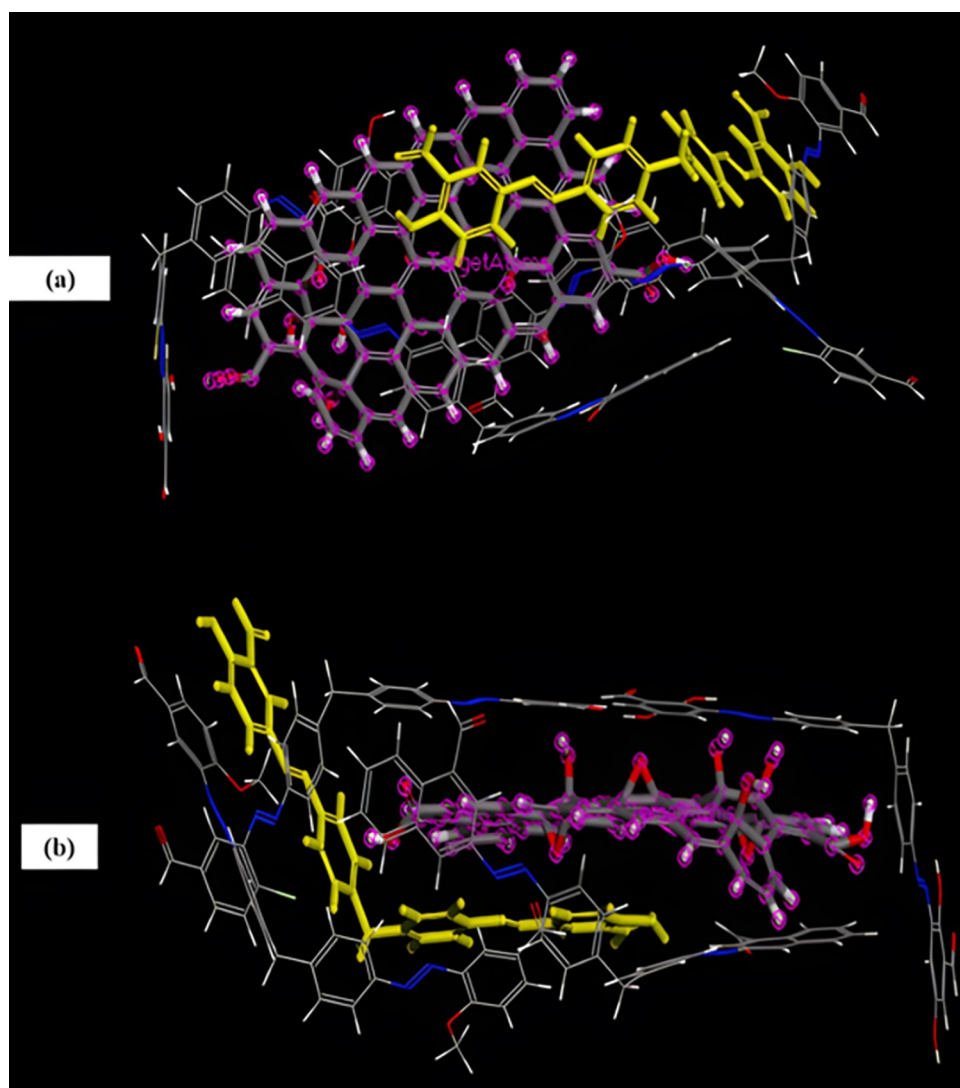


Fig 12. Adsorption complex of organic dyes and GO (HT-4 is shown in yellow color; a and b are top and side views, respectively).

<https://doi.org/10.1371/journal.pone.0299364.g012>

found to be intermolecular hydrogen bonding and π - π interactions. Tabular values of DE_{ad}/dNi shows that greater amount of energy i.e., -67.5352 Kcal/mol is required to separate HT-4 from GO as compared to other dyes because of its stronger adsorption with adsorbent surface thereby indicating greater effectiveness of GO in removal of HT-4.

4. Conclusions

Herein, we explored the adsorption of five novel azodyes onto the surface of GO through a combination of experimental UV-Vis spectroscopic method and computational DFT and Monte Carlo methods. We systematically investigated the adsorption of azo-dyes on GO, considering adsorbent dosage, contact time, and the Langmuir adsorption isotherm. The experimental data were explained by the Langmuir isotherm model, and the adsorption kinetics was modeled successfully by pseudo-second-order rate equation.

Computational DFT and Monte Carlo results revealed a predominantly physisorption nature in the adsorption process of azo-dyes on GO. The negatively charged surface, decorated with oxide functional groups, exhibited higher adsorption of HT-4 compared to other azodyes. Non-covalent and charge interactions were identified as driving forces for the adsorption on GO. Electronic and thermodynamic parameters calculated through DFT and MC simulation confirmed favorable adsorption of all azodyes, HT-4 being most efficient to be adsorbed on GO surface as revealed by its lowest ΔE_{ads} . Both experimental and computational findings, particularly thermodynamic parameters, were mutually supportive. The physisorption depicted reusability and potential of GO as an effective adsorbent for removing these novel azo dyes from aqueous solutions. Our results contribute to the development of efficient adsorbents for the broader removal of dyes in water purification applications.

Supporting information

S1 Fig. (a-e) FT-IR, XRD, TGA, SEM, and UV-spectra, respectively, of GO. **(f)** FTIR of recycled GO.

(TIF)

S2 Fig. IR and NMR spectra of HT-2.

(TIF)

S1 Table. Supporting information data for pseudo-first-order and pseudo-second-order kinetic modeling of azo-dyes adsorption on GO.

(XLSX)

S1 Scheme. Synthesis of substituted Bis 3, 3'-(4, 4'-diazenyldiphenylmethane) benzaldehydes.

(PNG)

S1 Graphical abstract.

(TIF)

Acknowledgments

Authors Acknowledge School of Interdisciplinary Engineering & sciences (SINES), National University of Sciences and Technology (NUST), for providing supercomputer and computational facilities. Co-author Dr. Irfan Ahmad extends his appreciation to the Deanship of Scientific Research at King Khalid University for funding through the Small Group Research Project under grant #(RGP/1/38/44).

Author Contributions

Conceptualization: Fouzia Perveen, Zoniya Arshad.

Data curation: Haris bin Tanveer.

Formal analysis: Hummera Rafique.

Investigation: Haris bin Tanveer, Fouzia Perveen, Nasima Arshad.

Methodology: Haris bin Tanveer, Sumaiya Azam.

Software: Fouzia Perveen, Sumaiya Azam.

Supervision: Fouzia Perveen.

Validation: Haris bin Tanveer, Sumaiya Azam, Sher Qadar.

Visualization: Haris bin Tanveer, Salman u Zaman.

Writing – original draft: Haris bin Tanveer, Nasima Arshad.

Writing – review & editing: Ahmad Irfan.

References

1. Mondal S., "Methods of dye removal from dye house effluent—An overview," *Environ. Eng. Sci.*, vol. 25, no. 3, pp. 383–396, 2008, <https://doi.org/10.1089/ees.2007.0049>
2. Rastogi K., Sahu J. N., Meikap B. C., and Biswas M. N., "Removal of methylene blue from wastewater using fly ash as an adsorbent by hydrocyclone," *J. Hazard. Mater.*, vol. 158, no. 2–3, pp. 531–540, 2008, <https://doi.org/10.1016/j.jhazmat.2008.01.105> PMID: 18339480
3. Wang L., Zhang J., and Wang A., "Removal of methylene blue from aqueous solution using chitosan-g-poly(acrylic acid)/montmorillonite superadsorbent nanocomposite," *Colloids Surfaces A Physicochem. Eng. Asp.*, vol. 322, no. 1–3, pp. 47–53, 2008, <https://doi.org/10.1016/j.colsurfa.2008.02.019>
4. Puvaneswari N., Muthukrishnan J., and Gunasekaran P., "Toxicity assessment and microbial degradation of azo dyes," *Indian J. Exp. Biol.*, vol. 44, no. 8, pp. 618–626, 2006. PMID: 16924831
5. Chung K. T., "Azo dyes and human health: A review," *J. Environ. Sci. Heal.—Part C Environ. Carcinog. Ecotoxicol. Rev.*, vol. 34, no. 4, pp. 233–261, 2016, <https://doi.org/10.1080/10590501.2016.1236602> PMID: 27635691
6. Tehrani-Bagha A. R., Nikkar H., Mahmoodi N. M., Markazi M., and Menger F. M., "The sorption of cationic dyes onto kaolin: Kinetic, isotherm and thermodynamic studies," *Desalination*, vol. 266, no. 1–3, pp. 274–280, 2011, <https://doi.org/10.1016/j.desal.2010.08.036>
7. Crini G., "Non-conventional low-cost adsorbents for dye removal: A review," *Bioresour. Technol.*, vol. 97, no. 9, pp. 1061–1085, 2006, <https://doi.org/10.1016/j.biortech.2005.05.001> PMID: 15993052
8. Ma J. et al., "Enhanced adsorptive removal of methyl orange and methylene blue from aqueous solution by alkali-activated multiwalled carbon nanotubes," *ACS Appl. Mater. Interfaces*, vol. 4, no. 11, pp. 5749–5760, 2012, <https://doi.org/10.1021/am301053m> PMID: 23062571
9. Ramesha G. K., Vijaya Kumara A., Muralidhara H. B., and Sampath S., "Graphene and graphene oxide as effective adsorbents toward anionic and cationic dyes," *J. Colloid Interface Sci.*, vol. 361, no. 1, pp. 270–277, 2011, <https://doi.org/10.1016/j.jcis.2011.05.050> PMID: 21679961
10. Sharma P., Hussain N., Borah D. J., and Das M. R., "Kinetics and adsorption behavior of the methyl blue at the graphene oxide/reduced graphene oxide nanosheet-water interface: A comparative study," *J. Chem. Eng. Data*, vol. 58, no. 12, pp. 3477–3488, 2013, <https://doi.org/10.1021/je400743r>
11. Yan H. et al., "Effects of the oxidation degree of graphene oxide on the adsorption of methylene blue," *J. Hazard. Mater.*, vol. 268, pp. 191–198, 2014, <https://doi.org/10.1016/j.jhazmat.2014.01.015> PMID: 24491443
12. Sarkar C., Bora C., and Dolui S. K., "Selective dye adsorption by pH modulation on amine-functionalized reduced graphene oxide-carbon nanotube hybrid," *Ind. Eng. Chem. Res.*, vol. 53, no. 42, pp. 16148–16155, 2014, <https://doi.org/10.1021/ie502653t>
13. Kim H., Kang S. O., Park S., and Park H. S., "Adsorption isotherms and kinetics of cationic and anionic dyes on three-dimensional reduced graphene oxide macrostructure," *J. Ind. Eng. Chem.*, vol. 21, pp. 1191–1196, 2015, <https://doi.org/10.1016/j.jiec.2014.05.033>

14. Thangavel S. and Venugopal G., "Understanding the adsorption property of graphene-oxide with different degrees of oxidation levels," *Powder Technol.*, vol. 257, pp. 141–148, 2014, <https://doi.org/10.1016/j.powtec.2014.02.046>
15. Chigo Anota E., Hernández Cocolletzi H., and Rubio Rosas E., "LDA approximation based analysis of the adsorption of O3 by boron nitride sheet," *Eur. Phys. J. D*, vol. 63, no. 2, pp. 271–273, 2011, <https://doi.org/10.1140/epjd/e2011-10608-4>
16. Johnson L. E. and Engel T., "Integrating computational chemistry into the physical chemistry curriculum," *J. Chem. Educ.*, vol. 88, no. 5, pp. 569–573, 2011, <https://doi.org/10.1021/ed900064n>
17. Bitounis D., Ali-Boucetta H., Hong B. H., Min D. H., and Kostarelos K., "Prospects and challenges of graphene in biomedical applications," *Adv. Mater.*, vol. 25, no. 16, pp. 2258–2268, 2013, <https://doi.org/10.1002/adma.201203700> PMID: 23494834
18. A Abdala A., "Applications of Graphene in Catalysis," *J. Biofertilizers Biopestic.*, vol. 05, no. 01, 2014, <https://doi.org/10.4172/2157-7544.1000132>
19. Konicki W., Aleksandrak M., Moszyński D., and Mijowska E., "Adsorption of anionic azo-dyes from aqueous solutions onto graphene oxide: Equilibrium, kinetic and thermodynamic studies," *J. Colloid Interface Sci.*, vol. 496, pp. 188–200, 2017, <https://doi.org/10.1016/j.jcis.2017.02.031> PMID: 28232292
20. Chung K. T., "The significance of azo-reduction in the mutagenesis and carcinogenesis of azo dyes," *Mutat. Res. Genet. Toxicol.*, vol. 114, no. 3, pp. 269–281, 1983, [https://doi.org/10.1016/0165-1110\(83\)90035-0](https://doi.org/10.1016/0165-1110(83)90035-0) PMID: 6339890
21. King-Thom Chung C. E. C., "Mutagenicity of azo dyes: Structure-activity relationships," *Mutat. Res.*, vol. 277, pp. 201–220, 1992. [https://doi.org/10.1016/0165-1110\(92\)90044-a](https://doi.org/10.1016/0165-1110(92)90044-a) PMID: 1381050
22. Salahshoori I., Namayandeh Jorabchi M., Ghasemi S., Golriz M., Wohlrab S., and Khonakdar H. A., "Advancements in wastewater Treatment: A computational analysis of adsorption characteristics of cationic dyes pollutants on amide Functionalized-MOF nanostructure MIL-53 (Al) surfaces," *Sep. Purif. Technol.*, vol. 319, no. February, p. 124081, 2023, <https://doi.org/10.1016/j.seppur.2023.124081>
23. Zaaba N. I., Foo K. L., Hashim U., Tan S. J., Liu W. W., and Voon C. H., "Synthesis of Graphene Oxide using Modified Hummers Method: Solvent Influence," *Procedia Eng.*, vol. 184, pp. 469–477, 2017, <https://doi.org/10.1016/j.proeng.2017.04.118>
24. Liu L., Luo X. B., Ding L., and Luo S. L., Application of Nanotechnology in the Removal of Heavy Metal From Water. Elsevier Inc., 2018. <https://doi.org/10.1016/B978-0-12-814837-2.00004-4>
25. Franchini M., Philippsen P. H. T., and Visscher L., "The becke fuzzy cells integration scheme in the amsterdam density functional program suite," *J. Comput. Chem.*, vol. 34, no. 21, pp. 1819–1827, 2013, <https://doi.org/10.1002/jcc.23323> PMID: 23720371
26. Perdew J. P., "Density-functional approximation for the correlation energy of the inhomogeneous electron gas," *Phys. Rev. B*, vol. 46, no. 6, pp. 3601–3631, 1991, <https://doi.org/10.1103/PhysRevB.46.3601> PMID: 900728
27. Becke A. D., "Density-functional exchange-energy approximation with correct asymptotic behavior," *Phys. Rev. A*, vol. 38, 1988, <https://doi.org/10.1103/physreva.38.3098> PMID: 9900728
28. Kumar R. et al., "Recent advances on water disinfection using bismuth based modified photocatalysts: Strategies and challenges," *J. Clean. Prod.*, vol. 297, p. 126617, 2021, <https://doi.org/10.1016/j.jclepro.2021.126617>
29. Soni V. et al., "Fabricating cattle dung-derived nitrogen-doped biochar supported oxygen-deficient ZnO and Cu2O-based novel step-scheme photocatalytic system for aqueous Doxycycline hydrochloride mitigation and Cr (VI) reduction," *J. Environ. Chem. Eng.*, vol. 11, no. 5, p. 110856, 2023, <https://doi.org/10.1016/j.jece.2023.110856>
30. Sharma K. et al., "Recent progress on MXenes and MOFs hybrids: Structure, synthetic strategies and catalytic water splitting," *Int. J. Hydrogen Energy*, vol. 48, no. 17, pp. 6560–6574, 2023, <https://doi.org/10.1016/j.ijhydene.2022.01.004>
31. Omar A. Z., El-Rahman M. A., Hamed E. A., El-Sadany S. K., and El-atawy M. A., "Synthesis, spectroscopic characterization and dyeing performance of novel bis azo dyes derived from benzidine," *Sci. Rep.*, vol. 13, no. 1, pp. 1–14, 2023, <https://doi.org/10.1038/s41598-023-34660-4> PMID: 37188698
32. Fakhri A., "Adsorption characteristics of graphene oxide as a solid adsorbent for aniline removal from aqueous solutions: Kinetics, thermodynamics and mechanism studies," *J. Saudi Chem. Soc.*, vol. 21, pp. S52–S57, 2017, <https://doi.org/10.1016/j.jscs.2013.10.002>
33. Tanyildizi M. Ş., "Modeling of adsorption isotherms and kinetics of reactive dye from aqueous solution by peanut hull," *Chem. Eng. J.*, vol. 168, no. 3, pp. 1234–1240, 2011, <https://doi.org/10.1016/j.cej.2011.02.021>
34. "Zur Theorie der sogenannten Adsorption gelöster Stoffe," *Zeitschrift für Chemie und Ind. der Kolloide*, vol. 2, no. 1, pp. 15–15, 1907, <https://doi.org/10.1007/bf01501332>